C. R. Physique 16 (2015) 227–240

Contents lists available at ScienceDirect

Comptes Rendus Physique

www.sciencedirect.com

Multiferroic materials and heterostructures / Matériaux et hétérostructures multiferroïques

Domains and domain walls in multiferroics

Domaines et parois de domaines dans les multiferroïques

Sylvia Matzen [a], Stéphane Fusil [b,*]

[a] *Institut d'électronique fondamentale, Bat. 220, Université Paris-Sud, UMR 8622, CNRS, 91405 Orsay, France*
[b] *Unité mixte de physique CNRS/Thales, campus de l'École polytechnique, 1, avenue Augustin-Fresnel, 91767 Palaiseau, France*

ARTICLE INFO

Article history:
Available online 9 March 2015

Keywords:
Multiferroics
Ferroelectricity
Ferromagnetism
Domains
Domain walls
Magnetoelectric coupling

Mots-clés :
Multiferroïques
Ferroélectricité
Ferromagnétisme
Domaines
Parois de domaine
Couplage magnétoélectrique

ABSTRACT

Multiferroics are gathering solid-state matter in which several types of orders are simultaneously allowed, as ferroelectricity, ferromagnetism (or antiferromagnetism), ferroelasticity, or ferrotoroidicity. Among all, the ferroelectric/ferromagnetic couple is the most intensively studied because of potential applications in novel low-power magnetoelectric devices. Switching of one order thanks to the other necessarily proceeds via the nucleation and growth of coupled domains. This review is an introduction to the basics of ferroelectric/ferromagnetic domain formation and to the recent microscopy techniques devoted to domains imaging, providing new insights into the archetypal multiferroic domain morphologies. Some relevant examples are also given to illustrate some of the unexpected properties of domain walls, as well as the way these domain walls can be manipulated altogether thanks to various types of magnetoelectric coupling.

RÉSUMÉ

Les multiferroïques rassemblent les solides qui permettent la cohabitation de plusieurs ordres ferroïques tels que la ferroélectricité, le ferromagnétisme (ou l'antiferromagnétisme), la ferroélasticité ou la ferrotoroïdicité. Parmi ces ordres, le couple ferroélectrique/ferromagnétique est celui qui permet d'envisager le plus directement la réalisation de dispositifs originaux dans lesquels, par exemple, l'aimantation peut être renversée par l'application d'un champ électrique, par simple application d'une tension et avec un faible coût énergétique. La manipulation d'un ordre par un autre doit opérer par nucléation et croissance de domaines nécessairement couplés. Cette revue introduit les mécanismes gouvernant la formation de ces domaines et les techniques les plus récentes pour leur observation à l'échelle microscopique, donnant ainsi accès aux morphologies les plus typiques de domaines multiferroïques. Quelques exemples parmi les plus significatifs permettront d'illustrer les propriétés spécifiques liées aux parois de ces domaines, ainsi que la façon dont ces parois peuvent être manipulées les unes par l'intermédiaire des autres grâce à différents types de couplage magnétoélectrique.

* Corresponding author.
E-mail address: stephane.fusil@thalesgroup.com (S. Fusil).

http://dx.doi.org/10.1016/j.crhy.2015.01.013
1631-0705/

The renewed interest in multiferroics and magnetoelectric coupling is largely associated with non-volatile memory applications. The maturity of MRAMs and FeRAMS allows devices to be on the market and their "all-in-one" magneto-electric extensions are envisaged in the same application line. The memory function is on sight and the information is conceived to be encoded thanks to the electric *and* magnetic orders. Expected devices are for example aiming at taking advantages of both ferromagnetic (FM) and ferroelectric (FE) orders without their respective drawbacks, exploiting the easy "write" of FE along with the mastered "read" of FM. The binary operation is here implicit, with complete switching of one order thanks to the other. As the switching is governed by the nucleation and the propagation of domain walls (either FE or FM, eventually coupled one with the other), these objects have promoted a flurry of activity in the scientific community. Their dynamic behavior is directly related to the switching speed and their potential pinning is a serious cause for fatigue, two key issues for applications. Moreover, functionalities can still exist even if the device is not spatially fully saturated, i.e. domains of different orientations coexist with their associated domain walls. Here again, the binary memory function can be on sight. The most archetypal example is the racetrack memory proposed by Parkin [1]: spin polarized electric currents are used to push magnetic domain walls along a permalloy wire; and each magnetic domain corresponds to a bit electrically driven to flow under the read/write elements. A wider playground is provided by FE and/or FM domains in multiferroics, allowing more exotic concepts of devices to emerge. For instance, the revival of analogic components for neuromorphic computing architectures is epitomized in the "memristor". A memristor is a variable resistance that depends on its current history and mimics the synapse function of the brain. Several memristors concepts have been explored and fully electronic examples are given by the spintronic [2] and the ferroelectric memristors [3]. In both cases, the final resistance of the FM or FE media is governed by the relative proportion of domain populations (FM or FE). The ability to tune the device resistance is related to the domain wall kinetic and domain stability. Even more original concepts can be envisaged if the device functionality is no more localized in the domains but in the domain walls. Intrinsic properties of domain walls are indeed different from the ones of the parent domains as the local symmetry at the walls is different from the bulk one. Various interfacial phenomena can arise in these nanoscale objects, leading for example to domain wall conductivity [4], magnetotransport [5], or photovoltaic response [6] (see Section 2). In multiferroic single crystals and thin films, different mechanisms can contribute to the formation of ferroelectric and magnetic domains, and a large variety of domain walls architectures has been observed. These observations are the prerequisite for novel functionalities of electronic devices. This article is focused on recently reported results about domains and domain walls in different types of multiferroic materials, especially the room temperature multiferroic $BiFeO_3$ (BFO) and rare earth hexagonal manganites RE–MnO_3 (RE = Y, Er, Ho).

1. Domain structures in multiferroic materials

Ferroics spontaneously divide into small regions of different polarity, called "domains", while the boundaries between adjacent domains are called "domain walls" or "domain boundaries". In this section, the driving force for domain formation is presented with a review of the different domain topologies reported in multiferroics.

1.1. Formation of domains

In any ferroic materials, the presence and size of domains (and therefore the density of domain walls) depends on their boundary conditions. Self-induced depolarizing fields appear when the polarization has a component perpendicular to the material's surface, and cannot be perfectly screened. In addition, residual stresses caused by epitaxy, shape anisotropy or structural defects induce domains in most multiferroics. The domain size is determined by the competition between the domains energy (increasing with size) and the energy penalty needed to create the domain walls. For instance, in ferroelectrics, smaller domains have smaller depolarizing and elastic energies, but the energy gain by reducing domain size is balanced by the increasing number of domain walls. This leads to the well-known square root dependence of the domain size as a function of the film thickness or Kittel's law [7]. Similarly in ferromagnets, uniform magnetization does not correspond to the energy optimum. The domain structure is the result of the competition between the anisotropy energy due to the spins in the domain wall (which are no longer aligned along the easy axis) and the exchange energy between domains of different magnetization. The similarities are striking, even if ferromagnetic domain sizes are generally larger than ferroelectric ones for a given thickness. The size of the domain wall itself is also different in both kinds of systems: ferroelectric domain walls are only a few nm large (from Landau–Ginzburg–Devonshire theory as well as from transmission electron microscopy observation), while magnetic domain walls are one order of magnitude larger (as determined by the balance between the exchange energy and the magnetic anisotropy). Both kinds of domain walls are nevertheless observed to be coinciding in some multiferroics and one type of domain walls can be manipulated thanks to the other type (see Section 3).

Kittel's law has been extended to ferroelastic thin films epitaxially strained [8], to ferroelectric epitaxial thin films [9–11] and to magnetoelectric multiferroics [12]. The square root dependence of domains width with film thickness appears to be a general property of ferroics and holds over a remarkable range of sizes and shapes. This global trend is observed even if growth and boundary conditions are obviously key issues. For instance, in the most studied multiferroic, namely $BiFeO_3$ with coexistence of ferroelectric and antiferromagnetic orders at room temperature, the ferroelectric domain structure can be "mosaic like" for higher growth rates or "stripe like" for lower growth rates closer to thermodynamic equilibrium (Fig. 1b

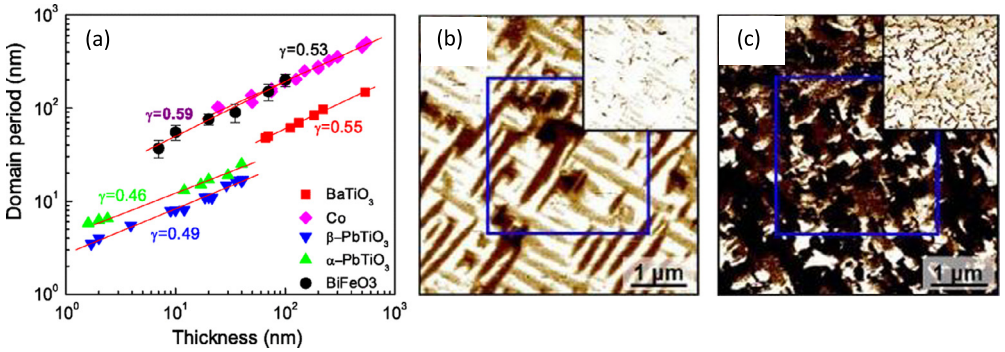

Fig. 1. (Color online.) (a) Domain size as a function of thickness in prototypical ferroelectrics ($BaTiO_3$, $PbTiO_3$) compared with the ferroelectric domain size in the multiferroic $BiFeO_3$. $BiFeO_3$ exhibits "larger" FE domains, in line with FM domain size in standard ferromagnets (Co); after Catalan et al. [26]. (b) and (c) In plane PFM images showing "stripes like" and "bubble like" FE domain structure in $BiFeO_3$ thin films grown respectively at low (∼0.1–0.3 Å/s) and high (∼1–2 Å/s) rates; after Martin et al. [14].

and c). Among the height possible variants of the FE polarization (pointing along the height different {111} directions), some variants can be preferred depending on various parameters such as

i) the growth conditions (growth mode with step bunching or step flow [13], and growth speed [14])
ii) the screening boundary conditions (ultra high vacuum or ambient for the top surface; carrier density of the bottom electrode [15])
iii) the substrate induced symmetry mismatch [16] or the substrate miscut angle [17].

Ultrathin films or nano-objects are questioning the universality and limits of Kittel's law, as discussed in many studies [18–25]. Kittel's law is observed to be globally valid for multiferroics, even if the ferroelectric domain size can be shifted toward higher values, matching the regular size of ferromagnetic domains [26] (Fig. 1a).

1.2. Observation of domains

The observation and study of FM and FE domains is strained by the progress made in imaging techniques with the required spatial resolution and sensitivity. An additional degree of complexity is intrinsic to multiferroics as FM and FE contributions have both to be distinguished. Most of the available microscopy techniques are simultaneously sensitive to the FE *and* to the FM orders, giving rise to cross talks between those two contrasts. For instance, Photo Emission Electron Microscopy (PEEM) based on X-ray linear dichroism feels the asymmetry of the electronic charge distribution which is dependent on the FE domains pattern and also on the antiferromagnetic one. Another example is given by Atomic Force Microscopy (AFM) for which a magnetized tip feels the magnetic stray field as well as the unscreened electric stray field induced by FE surface charges. In the following, some examples of relevant approaches are given to illustrate how both FE and FM domains can be successfully distinguished in intrinsic multiferroics or in artificial multiferroics stacks (FM on FE and vice versa).

i) Optical microscopy (Kerr and birefringent)

Bulk crystals are convenient for imaging as their pristine domain size is larger than in thin films or in nano-objects. If the domain size is big enough to be resolved by optical microscopy, FE domains are revealed by birefringent contrast, while FM domains are visible thanks to magneto-optical Kerr contrast. A crystal clear example is given by Lahtinen and co-workers [27,28] in a FE/FM heterostructure for which the two components coupling can be mediated by strain, exchange, or charge [29]. A thin film of $Co_{0.6}Fe_{0.4}$ (15 nm) is deposited on top of a $BaTiO_3$ crystal and is semi-transparent for this range of thickness. The FM domains of the $Co_{0.6}Fe_{0.4}$ magnetic layer are observed to perfectly match the FE domains in $BaTiO_3$ (Fig. 2a and b). In this case, the full imprinting is attributed to strain effect of different types of FE domains affecting the uniaxial anisotropy of the FM layer by inverse magnetostriction.

ii) Atomic Force Microscopy

Atomic Force Microscopy (AFM) allows one operation mode dedicated to magnetic contrast, namely Magnetic Force Microscopy (MFM); and one other mode devoted to ferroelectric contrast, namely Piezoresponse Force Microscopy (PFM). The MFM magnetized tip experiences attracting or repelling forces depending on its own magnetization relative to the sample one. This force induces a phase lag for the tip oscillation and MFM phase images illustrate the magnetic stray field of the multiferroic. Magnetic tips are actually coated by metallic ferromagnetic materials, so that they are conducting and can then

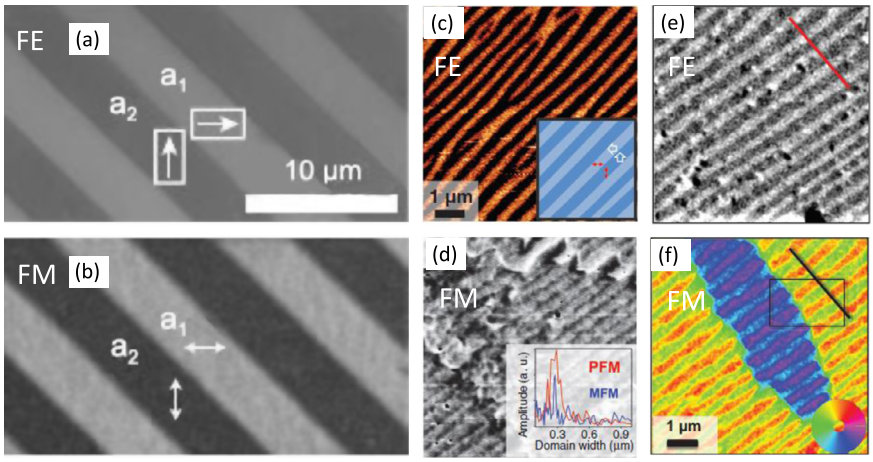

Fig. 2. (Color online.) Ferroelectric/magnetic bilayers (CoFe/$BaTiO_3$ and CoFe/$BiFeO_3$). $Co_{0.6}Fe_{0.4}$/$BaTiO_3$ with ferroelastic coupling: Polarization microscopy images of the ferroelectric (a) and ferromagnetic (b) domain structures. The arrows indicate the polarization direction in the BTO substrate and the orientation of the uniaxial magnetic easy axes in the CoFe film deposited on top; after Lahtinen et al. [28]. $Co_{0.9}Fe_{0.1}$/$BiFeO_3$ with interfacial exchange coupling: PFM image showing the FE stripes like domains in $BiFeO_3$ (c). MFM image of the $Co_{0.9}Fe_{0.1}$ on top with stripe like magnetic contrast of the same periodicity (d). Backscattered electron contrast imaging of the FE domains in $BiFeO_3$ (e) and scanning electron microscopy with polarization analysis (SEMPA) showing the imprinted FM domains in $Co_{0.9}Fe_{0.1}$ (f); after Trassin et al. [30].

also be used for PFM imaging. PFM takes advantage from the fact that each ferroelectric material is also piezoelectric. By applying an alternating bias at a given frequency between the conducting tip lying on top of the multiferroic and a bottom electrode, the material is forced to vibrate at the same frequency thanks to the converse piezoelectric effect. The phase lag between the electric excitation and the piezoelectric vibration is related to the local direction of the polarization, producing the ferroelectric contrast. The resolution for both types of microscopy is a few nanometers. An example is given in Fig. 2c and d, where MFM contrast coming from a $Co_{0.9}Fe_{0.1}$ amorphous alloy (2.5 nm thickness) is correlated with the PFM contrast coming from the underneath $BiFeO_3$ FE domains [30]. In this configuration, the FE induced charges are screened by the magnetic top electrode and the MFM signal is pure. This correlation attests for the coupling between the CoFe ferromagnetic moments and the antiferromagnetic domains in $BiFeO_3$, the latter being magneto-electrically coupled with the FE order.

iii) Scanning Electron Microscopy

Scanning Electron Microscopy with Polarization Analysis (SEMPA) detects the spin polarization of secondary electrons [31]. This spin polarization reflects the net spin density at the Fermi level in the magnetic material, and the local surface's magnetic orientation with a resolution of about ten nanometers. The same electron microscope is also able to distinguish the different ferroelectric variants thanks to the different electric field landscapes experienced by back-scattered electrons before reaching the detector. The resolution is then again a few or a few tens of nanometers. SEMPA is then able to give the full picture of FM and FE domains within the same experimental setup. The very same system as already mentioned above ($Co_{0.9}Fe_{0.1}$ on top of $BiFeO_3$) illustrates the perfect matching between the FM domains imprinted by the underneath FE domains, as can be seen in Fig. 2e and f from [30].

iv) Photo Emission Electron Microscopy (PEEM)

A possible way to discriminate the FM/FE contrasts is to take advantage of the potentially different Curie and Néel temperatures of the multiferroic. This approach was used by Zhao et al. [32] to discriminate the antiferromagnetic contribution and the ferroelectric one in PEEM images of $BiFeO_3$ thin films. Careful comparison of PEEM contrast under and above the Néel temperature of $BiFeO_3$ (640 K) allows us to separate the "pure" FE contrast from the multiferroic one. When possible, a smart combination of XMLD and XMCD-PEEM imaging (mapping spin and orbital magnetic moments) is a very powerful tool.

1.3. Peculiar domain morphologies: vertices and topological defects

Stripe and mosaic like domains are the most common and conceptually the simplest domain morphology, but they are not exclusive of more complex domain structures [33]. The introduction of sub nanometer resolved techniques, especially transmission electron microscopy and atomic force microscopy with polarization sensitivity, has revealed the diversity and complexity of the domain's structures in ferroic materials.

Within the past decade, the existence of 1D topological defects, namely vortices and vertices, has been predicted in ferroelectrics as their dimensions are reduced [34–40]. These predictions have motivated experimental work aimed to reveal

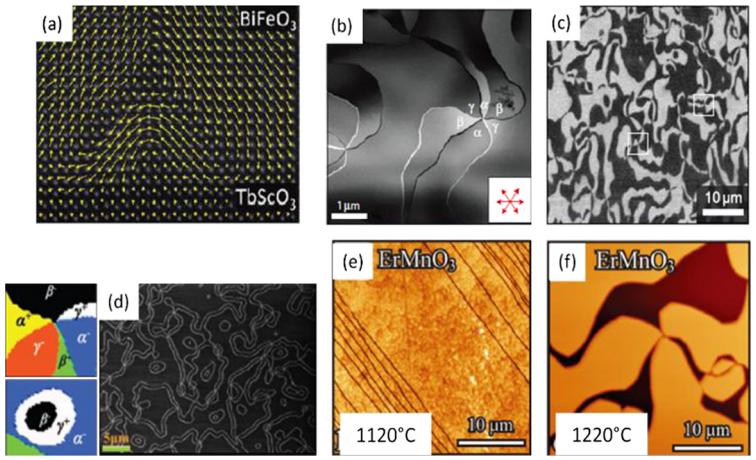

Fig. 3. (Color online.) Observation of topological defects in multiferroics. (a) Closure like polar arrangement at the junction between ferroelectric domain walls and an interface for $BiFeO_3$ thin films (TEM picture, adapted from Nelson et al. [51]). (b, c) Six-fold vertices in hexagonal multiferroic $YMnO_3$ single crystals, observed by TEM (b, adapted from Choi et al. [60]) and PFM (c, adapted from Jungk et al. [59]). (d) Coexistence of cloverleaf patterns and annular domains in annealed $ErMnO_3$ (SEM picture, adapted from Li et al. [65]) with the structural features and poling configuration for a vertex and an annular domain (left insets). (e, f) Thermal evolution of stripe domain into vertex–antivertex domain patterns in $ErMnO_3$ crystals annealed below (e) and above (f) the trimerization-structural transition temperature (AFM pictures of chemically etched crystals, adapted from Chae et al. [66]).

such complex topological arrangements of electrical dipoles. Vertices are topological singularities closely related to vortices. While a vortex requires flux closure, a vertex is just created at the intersection of domain walls. Some vertices can thus also be vortices, as for example the vertices induced by 90° closure quadrants. Several experimental studies have been focused on the effect of geometrical confinement on these nanoscale domain patterns [18,41], especially in thin lamellae and small-scale dots of ferroelectrics such as $BaTiO_3$ [24,25,42–44], $Pb[Zr_xTi_{1-x}]O_3$ [45] and $[Pb(Zn_{1/3}Nb_{2/3})O_3]_{(1-x)}[PbTiO_3]_{(x)}$ [46]. A few studies were also conducted on disk-shaped thin film capacitor structures of $Pb[Zr_xTi_{1-x}]O_3$ [47,48]. Recently, these complex domain structures have also been observed to occur spontaneously at grain boundaries and heterointerfaces in thin ferroelectric films of $Pb[Zr_xTi_{1-x}]O_3$ [49,50]. However, closure structures are difficult to observe in these conventional tetragonal ferroelectrics due to the high strain energy of such arrangement, so that ferroelastic stripes often appear within each quadrant to alleviate the stress.

Ferroelectric closure-like structure has been recently observed at heterointerfaces in multiferroic $BiFeO_3$ thin films [51,52]. In the work by Nelson et al., cross-sections of $BiFeO_3$ films have been studied nearby interfaces and clearly evidenced that depolarizing fields can induce polar rotation. At metallic interfaces offering charge compensation, simple stripe domains formed. At insulating interfaces offering poor screening, dipole reorientation was induced to reduce depolarizing fields, thus creating triangular domains with continuous polar rotation (Fig. 3a). Regular nanodomain vertex arrays have also been observed by TEM and PFM in $BiFeO_3$ single crystals [53].

1D topological defects have also been observed in hexagonal multiferroic manganites $REMnO_3$ (RE: rare earth, RE = Y, Er, Ho). In these improper ferroelectrics, the size mismatch between RE and Mn creates a trimerization-like structural phase transition, giving rise to ferroelectricity [54,55]. At lower temperature, ∼100 K, an antiferromagnetic ordering of Mn spins emerges and the ferroelectric domain walls tend to pin antiferromagnetic domain boundaries, indicating the presence of a magnetoelectric coupling [56,57]. In these materials, ferroelectric polarization and magnetization are coupled to the structural order parameter [58], giving rise to topological defects with unconventional functionalities (see Section 2). In $REMnO_3$, the structural phase transition leads to three antiphase domains (α, β, γ) supporting two directions of ferroelectric polarization (+, −). Cycles through all six domain configurations in cloverleaf arrangements have been visualized at the intersection of antiphase and ferroelectric domains. Cloverleaves can be viewed as vertices and antivertices, in which the cycle of domain configuration is reversed. These six-state vertices have been observed by TEM and PFM in $YMnO_3$ single crystals [59–61] (Fig. 3b and c), where the sign of electric polarization changes six times around the vertex core. Similar arrangements of topological six-fold vertices and antivertices have also been visualized in hexagonal $ErMnO_3$ single crystals [62–66]. The detailed structure of the domain walls in hexagonal manganites has been elucidated by first-principles electronic structure calculations [67], explaining why ferroelectric domain walls are always simultaneously antiphase walls. While the formation of six-fold topological defects is experimentally reported in many studies [59–64], the calculated lowest energy domain walls are predicted to form stripe domains. Two recent studies have proven a coexistence of annular domains [65] and stripe domains [66] with cloverleaf vertices in $REMnO_3$, influenced by slow kinetics and pinning. Thermal annealing experiments have directly shown that both annular and stripe domains can change into cloverleaf vertices above the trimerization-structural transition temperature, in agreement with stripe domain patterns being the true ground state in hexagonal manganites [67] (Fig. 3d–f). Very recently, a vortex-to-stripe transformation has been observed by applying shear strain to crystals of h-$ErMnO_3$, showing the potential of mechanical control of topological defects [68].

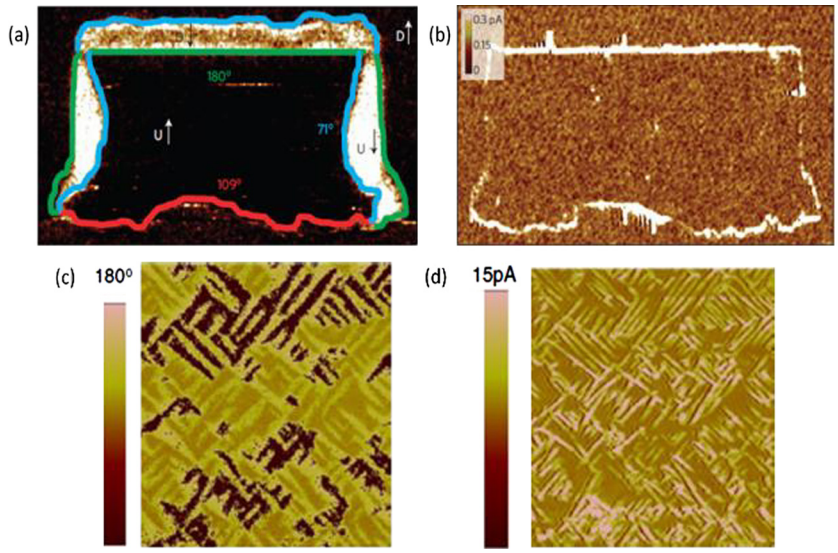

Fig. 4. (Color online.) Conductivity at domain walls in BFO thin films at room temperature. (a) In-plane PFM image and (b) corresponding conductive AFM image showing conduction at both 109° and 180° domain walls and absence of conduction at 71° domain walls in a BFO thin film (after Seidel et al. [4], pictures size = 6.4 × 3.5 μm^2). Conduction at both 71° and 109° domain walls in BFO thin films (after Farokhipoor et al. [75]), related to migration and accumulation of oxygen vacancy at the walls. (c) In-plane PFM picture and (d) conductive AFM picture (pictures size = 4 × 4 μm^2).

2. Properties of multiferroic domain walls and topological defects

This section is focused on some emergent properties at domain walls [18,69], in multiferroics that exhibit coupled order parameters. We present what is understood and what remains to be studied, in multiferroic BFO as well as in more recently investigated hexagonal manganites.

The idea that domain walls have their own symmetry and properties is straightforward: the properties that are allowed inside the domain walls can be predicted from the space group of the ferroic material. A net magnetization may appear inside the ferroelectric domain walls of multiferroics [70], as in $BiFeO_3$ where domain wall magnetization is allowed in the space group R3c.

2.1. Domain walls conductivity

In rhombohedral $BiFeO_3$ thin films, the ferroelectric domains have an insulating behavior, while significant conduction is evidenced at domain walls [4]. Seidel et al. were the first to observe that uncharged 109° and 180° domain walls in BFO thin films are conducting at room temperature, whereas no conduction is measured at the 71° domain walls (Fig. 4a and b). The origin of such conductivity at $BiFeO_3$ domain walls is controversial since many contributions can be involved, such as octahedral rotations, increased carrier density at the domain walls or electrostatic potential steps due to the in-plane polarization discontinuity. According to Seidel and co-workers, the observed conductivity is attributed to structurally induced changes in both electrostatic potential and local electronic structure, leading to a decrease of the band gap at the domain walls. These experimental results are supported by first-principle density-functional study of structural, electronic and magnetic properties of $BiFeO_3$ domain walls [70,71], calculating potential steps and reduced local band gaps at 109° and 180° walls, in agreement with the reported increased conductivity at both walls. These results stimulated much follow-on experimental work [72–78] to decipher the origins of the conductivity. In $YMnO_3$, the uncharged domain walls are less conducting than the domains [60], which is in exact opposite with $BiFeO_3$. The increase of the Y–O bond distance at domain walls could be responsible for the reduction of local conduction. It is worth noticing that while the high-temperature phase of BFO is more conducting than the ferroelectric phase [79], the converse effect is observed for $YMnO_3$. These results suggest that the properties of domain walls are similar to the properties of the material's paraphase: the insulating behavior of $YMnO_3$ domain walls is consistent with the insulating nature of $YMnO_3$ paraphase; the conducting state of the $BiFeO_3$ paraphase is consistent with the domain walls conductivity.

Defect accumulation at the walls is also expected to play a crucial role to control the transport properties. Interestingly, Farokhipoor et al. reported conductivity at both 71° and 109° domain walls in $BiFeO_3$ thin films [75] (Fig. 4c and d). Their temperature dependent studies revealed that the conduction for both domains and domain walls is governed by thermal activation of electrons from trap states at low voltages, and Schottky emission at higher voltages. The presence of a strain gradient at the ferroelastic domain walls was also proposed to encourage strain-driven migration of oxygen vacancies at the wall, inducing a decrease of the Schottky barrier of surface defect states and thus an enhancement of the conductivity at the domain walls [76]. The contribution of oxygen vacancies in the conduction of domain walls has also been studied

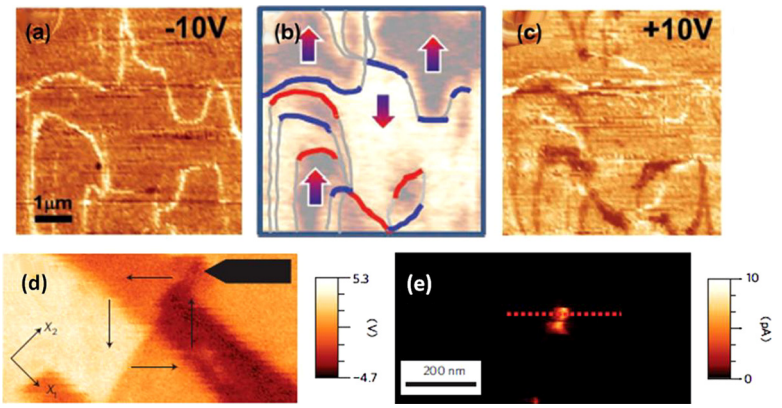

Fig. 5. (Color online.) Enhanced conduction at charged domain walls and topological defects. Conducting-AFM of domain walls on (110) surface in $HoMnO_3$, with forward bias (−10 V) (a), reverse bias (10 V) (c) and associated PFM picture (b) showing highly conductive tail-to-tail (blue lines), uncharged (gray lines) and less conductive head-to-head domain walls (red lines) (after Wu et al. [83]). In-plane PFM image of a vortex domain structure in BFO thin film (d) showing enhanced conductivity at the vortex core (c-AFM picture (e)) (after Balke et al. [77]).

in La-doped BFO films [72] having different oxygen vacancy concentrations thanks to annealing processes under different oxygen pressures. In this work, a tunable and thermally activated conductivity has been achieved at 109° domains walls. The conductivity could be modulated over an order of magnitude. In those studies, activation energies values were consistent with ionization of oxygen vacancy states [72,75,76]. Stolichnov et al. have recently evidenced persistent conductive paths even after erasing 109° domain walls in $BiFeO_3$, forming an electrical footprint of the initial domain walls [80]. These results epitomize the complexity of domain wall conduction. The mechanism giving rise to conduction, *i.e.* intrinsic (band gap reduction), or extrinsic (oxygen vacancies wall decoration), still is under debate. Migration and accumulation of oxygen vacancies at domain walls is nevertheless considered as the main cause for an observable increase of static conductivity, even if more complex phenomena cannot be excluded. Domain walls conduction is now observed in numerous standard ferroelectrics such as $Pb[Zr_xTi_{1-x}]O_3$ [81], $BaTiO_3$ [82], $LiNbO_3$ [78] and is not restricted to multiferroics.

Charged domain walls are energetically unfavorable and are rarely observed. However, in hexagonal manganites the domain walls are topologically protected and can become highly charged for specific orientations as for example in $HoMnO_3$ [83], and in $ErMnO_3$ [84]. Charged ferroelectric domain walls arise naturally from the topology of vortex–antivortex network in 3D crystals [59,62]. Unlike $BiFeO_3$, the family of multiferroic h-$REMnO_3$ materials provides thus a model system to study the conductivity of charged domain walls. Tail-to-tail domain walls on non-polar (110) surface in $HoMnO_3$ single crystals are observed to be more conductive for both bias signs, whereas head-to-head domain walls are less conductive at reverse bias (Fig. 5a–c). These phenomena can be explained by the attraction of mobile charge carriers with opposite sign. In p-type $HoMnO_3$, an enhanced conduction is obtained at tail-to-tail domain walls which attract holes, while the conduction is reduced at head-to-head domain walls which repel holes. The same type of conduction properties at 180° charged domain walls has also been reported in h-$ErMnO_3$. These studies also showed that positively charged domain walls (head-to-head) are wider than negatively charged domain walls (tail-to-tail) due to a larger screening length.

The functional properties of vertices are also under investigations. In the case of $BiFeO_3$, the conductivity of ferroelectric vortices is considerably higher than that of domain walls [77]. Fig. 5 displays the conductive AFM image of a vortex core in a BFO film, defined as the center of a closure domain formed by the in-plane polarization components of four head-to-tail domains. Enhanced conductivity is clearly observed at the vortex core (Fig. 5e), which shows the potential of ferroelectric vortices to be used as 1D conduction channels. Here again, the increased conductivity at vortex cores can be induced by changes of electronic structure due to the higher symmetry at these topological defects, and/or strain-driven charges carriers segregation and redistribution, as demonstrated by phase field modeling.

2.2. Domain walls magnetism

In addition to electrical conductivity, another interesting property that deserves intensive investigation is the magnetic behavior of multiferroic domain walls. Cross-coupling between coexisting magnetic and ferroelectric orders results in an appealing magnetoelectric coupling but is practically challenging since most multiferroics are antiferromagnets with vanishing magnetic moments. Visualizing cross-coupled domain walls in multiferroics is particularly interesting if the domain wall is found to escape from the antiferromagnetic nature of its parent material.

In $BiFeO_3$, the strength of the coupling between ferroelectric and antiferromagnetic walls has been extensively studied experimentally [32] and theoretically [71,85]. Recently, nanoscale phase boundaries in compressively strained BFO (exhibiting a mixture of rhombohedral-like phase embedded in tetragonal-like phase) have shown a remarkable enhancement of magnetism [86]. Imaging of structural and magnetic contrast by XMCD-PEEM strongly suggested that the enhanced magnetic moment in mixed-phase BFO films comes from the nanoscale phase boundaries (Fig. 6). The properties of multiferroic domain walls, such as magnetization and magnetoresistance [5], are now focusing intensive research.

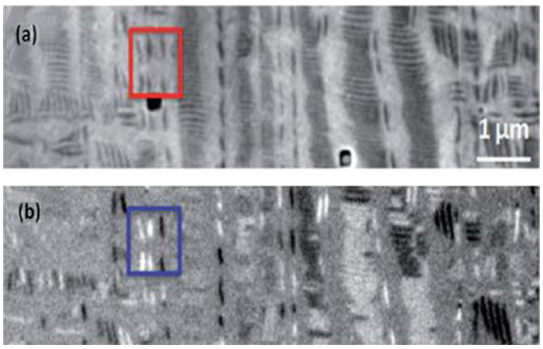

Fig. 6. (Color online.) Enhanced magnetism at nanoscale phase boundaries in mixed-phase BFO films (after Zhang et al. [86]). PEEM image with (a) structural contrast (R-like phase in dark stripes, T-like phase in bright stripes) and (b) magnetic contrast (magnetic moments pointing parallel and antiparallel relative to the incident X-rays, respectively in black and white contrast).

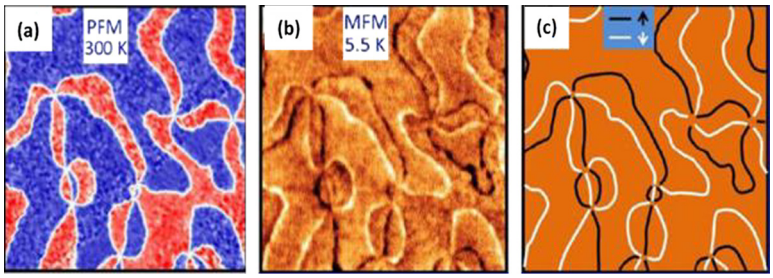

Fig. 7. (Color online.) Coupling between antiphase-ferroelectric and antiferromagnetic domain walls, creating alternating magnetic moments around vortex cores in a (001) $ErMnO_3$ single crystal (after Geng et al. [63]). (a) PFM image showing up (in red) and down (in blue) ferroelectric domains. (b) MFM image at the same location, with an associated cartoon (c) of the domain walls net up- (in black lines) and down- (in white lines) magnetic moment (pictures size $= 16 \times 16\ \mu m^2$). For interpretation of the references to color in this figure, the reader is referred to the online version of this article.

In hexagonal manganites, ferroelectric polarization and magnetization are coupled to the structural order parameter, leading to the clamping between ferroelectric and antiferromagnetic domain walls [56,57]. This clamping has been theoretically studied by Artyukhin et al. [58] and the authors showed that structural vortices in hexagonal manganites can induce magnetic ones so that ferroelectric domain walls can carry a magnetic moment. These results are consistent with a recent experimental report on collective magnetism around vortex cores in $ErMnO_3$ [63]. Using low-temperature magnetic force microscopy (MFM), alternating net magnetic moments have been evidenced at interlocked antiphase-ferroelectric domain walls around vortex cores (Fig. 7), creating a collective domain wall magnetism which can be controlled by a magnetic field. The authors suggested that this original domain wall magnetism could result from uncompensated Er^{3+} spins polarized by the Mn^{3+} antiferromagnetic order.

2.3. Other miscellaneous properties of domain walls

As presented before, structural changes at domain walls in BFO induce steps of the electrostatic potential and can thus affect the mechanism of charge separation. In conventional photovoltaic materials, electron-hole pairs are created by light absorption and separated by the electric field existing in the micrometer-thick depletion region. This mechanism necessarily limits the produced voltage to a maximum value equal to the material electronic band gap. In ferroelectric materials, an anomalous photovoltaic effect has been reported, giving rise to photovoltage values bigger than the band gap. This phenomenon is attributed to the FE polarization, inducing an internal electric field, and consequently a more efficient charge separation. Moreover, domain walls can act as nanoscale collectors of photovoltaic current, as reported by Seidel et al. [6]. The steps in the electrostatic potential can function to accumulate electrons and holes on opposite sides of the walls, so that photovoltages much higher than the band gap can be generated thanks to the addition of each photovoltage at periodically ordered domain walls.

Finally, another property of multiferroic domain walls is the possible enhancement of the piezoresponse, recently observed at phase boundaries in mixed-phase $BiFeO_3$ films [86] and at domain walls in hexagonal manganites [62].

Physics of domain walls in multiferroics is undoubtedly a growing field of interest. As device size is reduced, the density of domain walls increases, potentially affecting functional properties. Multiferroics are now envisaged to provide novel devices by exploiting the electrical conductivity and/or ferromagnetism of domain walls.

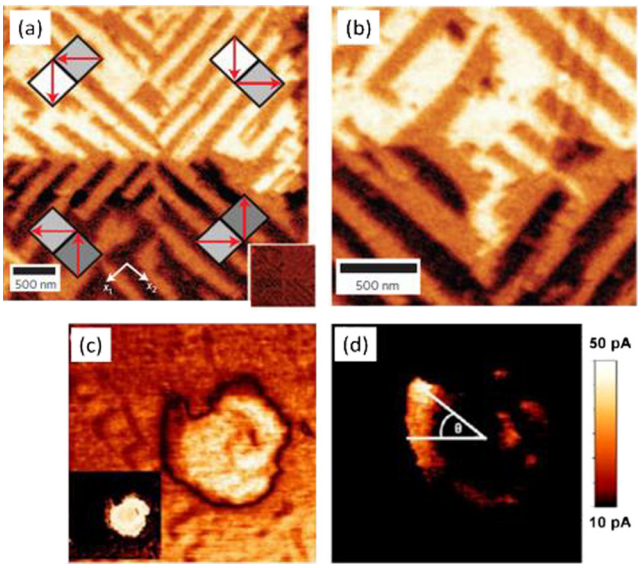

Fig. 8. (Color online.) Engineering domain patterns in BFO thin films by electric field. Creation of artificial star (a) and closure in-plane domains (b) by switching with a PFM tip (after Balke et al. [91]). PFM amplitude (c) and corresponding c-AFM picture (d) of a written circular domain pattern, showing the conduction modulation by wall geometry (after Vasudevan et al. [97]).

3. Manipulating domains and DW in multiferroics by external electric and/or magnetic fields

The coupling between the ferroelectric and the magnetic order in multiferroics should enable controlling magnetism by an electric field or controlling electrical polarization by a magnetic field, offering new perspectives for the development of functional electronic devices. A growing interest is being focused on multiferroic materials with spin-spiral structure [87,88], but the control of ferroelectricity (or magnetism) by a magnetic (or electric) field is limited to cryogenic temperatures. This mutual control motivates extensive search for novel multiferroic materials showing high magnetoelectric coupling at room temperature [89]. Until very recently, the only single-phase material displaying room temperature multiferroicity and magnetoelectric coupling was $BiFeO_3$, so that it is the most studied among multiferroics. Hexagonal ferrites, especially $LuFeO_3$ [90], are promising candidates for room temperature multiferroicity.

3.1. Manipulation of multiferroic domains by an electric field

When multiferroics are ferroelectrics, their domain structure can naturally be controlled by external electric fields. The development of atomic force microscopy provides the opportunity to apply electric fields to well-defined nanoscaled areas at will, allowing a deterministic control of the domain structure. It provides as a consequence an electrical low-power tuning of functional properties such as conduction or magnetism. Writing FE domains with desirable orientation relative to the polarization is possible thanks to the out-of-plane and in-plane electric fields available under a scanning probe. Domain walls can be positioned wherever needed and exotic topological defects can also be fabricated on demand. For example, Balke et al. [91] used scanning probe microscopy to 'write' specific dipole patterns, such as artificial star or flux-closure domain (Fig. 8a and b) in $BiFeO_3$ thin films. Controlling non-180° switching has been achieved thanks to the tip motion, and a local symmetry breaking of the rotationally invariant tip field. This technique has been further developed for the deterministic switching of polarization in ferroelectric thin films [92–94].

In order to use domain walls as functional elements, their conduction has to be controlled. Since conduction is strongly related to charges at walls [95,96], it is expected to be tuned by changing the charge profile along the domain wall. A significant variation in the current was indeed reported along the wall of a circular domain in $BiFeO_3$ film (Fig. 8c and d) nucleated by the microscope tip [97]. These results suggest that domain walls can be considered as dynamic tunable conductors. They could also offer a quasi-continuous spectrum of voltage tunable electronic states [73]. A deeper understanding and control of domain wall dynamics, nucleation and propagation under an electric field is necessary. The domain walls dynamics in magnetoelectric multiferroics still is an uncharted territory. The manipulation of ferroelectric domain walls is strongly affected by the presence of different types of defects [98], making the dynamics of coupled domain walls a complex mechanism that deserves intense investigation.

In $BiFeO_3$, antiferromagnetic domains are cross-coupled with ferroelectric domains. High-resolution images of both antiferromagnetic and ferroelectric domains in thin films have been obtained by co-localized PEEM and PFM [32]. A clear domain correlation is observed (Fig. 9) between antiferromagnetic and stripe ferroelectric domains. Ferroelectric domain switching is induced by electric field poling (Fig. 9d), and implies a switching of the antiferromagnetic order, clearly seen

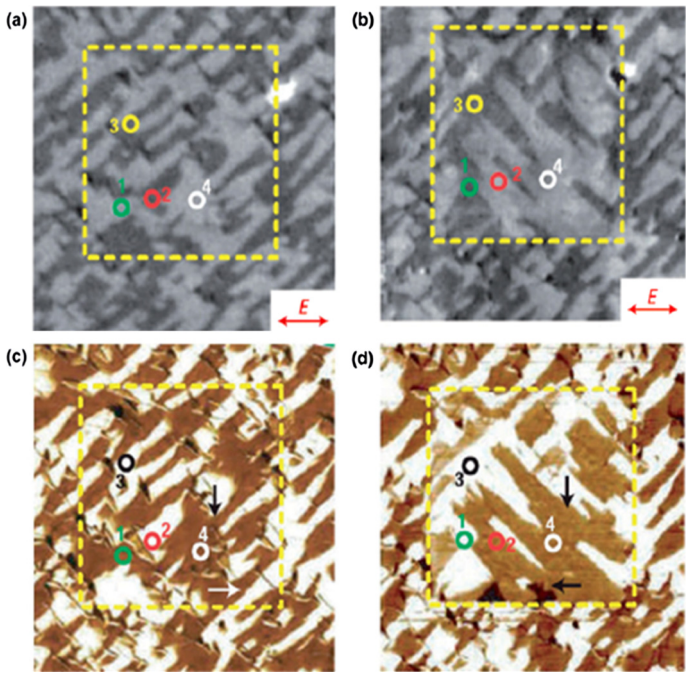

Fig. 9. (Color online.) Electrical control of antiferromagnetic domains in BFO films. PEEM images (a) before and (b) after electric poling, with the corresponding in-plane PFM images (c and d) showing the correlation between antiferromagnetic and ferroelectric domains, as well as the control of antiferromagnetic domains by electric field (after Zhao et al. [32], pictures size = 4 μm^2).

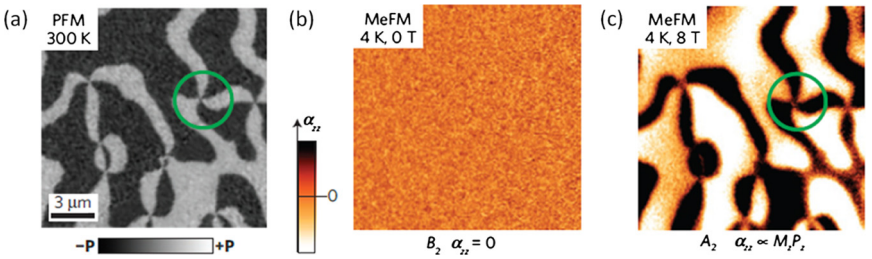

Fig. 10. (Color online.) Direct visualization of magnetoelectric domains in multiferroic $ErMnO_3$ single crystals. PFM (a) and MeFM (b, c) images at zero magnetic field (b) and 8.0 T (c), showing ferroelectric domains (a) with up (white) and down (dark) polarization and the effective magnetoelectric coupling coefficients α_{zz} (b, c) (after Geng et al. [64]).

from the contrast reversal in the PEEM images (Fig. 9b). Such electric-field control of magnetism has been studied in BFO crystals [99] and in thin films [100].

In hexagonal multiferroic manganites $REMnO_3$ (RE: rare earth, RE = Y, Er, Ho), ferroelectric polarization and magnetization are coupled to the structural order parameter [58], inducing a coupling between ferroelectric and magnetic domains [56,57]. Geng et al. have reported a direct visualization of magnetoelectric domains in multiferroic $ErMnO_3$ [64]. A magnetoelectric force microscopy technique (MeFM), combining magnetic force microscopy with in situ modulated electric field, was used to detect the E-induced magnetization and thus the magnetoelectric response of each multiferroic domains. Thanks to this technique, domains with different magnetoelectric coefficients can be visualized. MeFM measurements of $ErMnO_3$ at low temperature have revealed that the magnetoelectric domain pattern is identical to the ferroelectric one (Fig. 10), suggesting that the magnetoelectric coefficient is proportional to the product of the magnetization and the ferroelectric polarization along applied E-field direction. Unlike macroscopic measurements, which necessarily average the response due to the presence of domains, the MeFM technique offers a local detection of the magnetoelectric effect at the mesoscale. The dependence of magnetoelectric response with temperature and magnetic field also revealed a divergent effect near the tricritical point. This direct visualization of magnetoelectric domains at the mesoscale opens up investigation of emergent phenomena in multiferroic materials with coupled orders.

Another interesting experimental discovery has been reported by Seki et al. [101]. They observed by Lorentz transmission electron microscopy the formation of magnetoelectric skyrmions in an insulating magnet (Cu_2OSeO_3) and evidenced that skyrmion can magnetically induce electrical polarization. These results could pave the way toward the manipulation of skyrmions by an electric field without losses due to Joule heating.

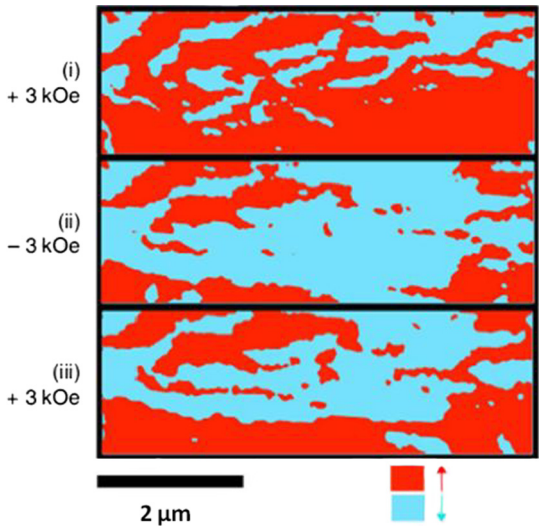

Fig. 11. (Color online.) Magnetic field control of ferroelectricity in ferromagnetic PZTFT solid solution. Lateral Piezoresponse Force Microscopy of a PZTFT lamella: cyan/red contrast discriminate the ferroelectric polarization directions pointing up/down. The images are acquired at remanence after applying a 3 kOe out of plane magnetic field (i) upward, (ii) downward and (iii) upward (after Evans et al. [102]).

3.2. Manipulation of multiferroic domains by a magnetic field

The newly discovered room-temperature multiferroic [$Pb(Zr,Ti)O_3$–$Pb(Fe,Ta)O_3$] (PZTFT) is, up to now, the only example of multiferroic offering magnetic field induced switching of ferroelectric domains [102,103]. Evans et al. observed a striking change (by almost 50%) of the relative proportion of different FE domains when applying a 3 kOe magnetic field in one or the opposite direction (Fig. 11). The coupling mechanism is assumed to be strain mediated but has to be further understood. These new candidate materials will definitely deserve extensive exploration in the future as genuine alternative multiferroics in order to provide a reciprocal control between ferroelectricity and magnetism.

3.3. Magnetoelectric coupling through ferroelectric/magnetic domains correlation in multiferroic heterostructures

As presented before, the magnetic order can be manipulated by an electric field in a multiferroic material thanks to the cross-coupling between ferroelectric and magnetic domains. However, the most serious impediment to the use of single phase multiferroics in devices remains the relatively weak magnetoelectric coupling and/or the quite low magnetic or ferroelectric critical temperatures. The scarcity of room temperature multiferroics is limiting the playground, mainly to antiferromagnetic/ferroelectric materials, such as $BiFeO_3$. Instead of using direct coupling between ferroelectric and ferromagnetic order parameters in a single-phase multiferroic material, another “two steps” approach is being investigated. This approach is based on indirect coupling through the intermediate antiferromagnetic order parameter. Two types of coupling phenomenon are then combined in heterostructures consisting of a ferromagnetic material in contact with a antiferromagnetic/ferroelectric multiferroic: the magnetoelectric coupling between antiferromagnetism and ferroelectricity in the multiferroic material allows an electric-field control of the antiferromagnetic order, and exploits in a second step the exchange interaction at the interface between the multiferroic antiferromagnet and the ferromagnet on top. The exchange coupling between the spins of the ferromagnet and the uncompensated spins at the interface of the antiferromagnetic multiferroic creates for instance the so-called exchange bias effect whose amplitude is determined by the size of antiferromagnetic domains [104], so the size of ferroelectric domains if coupled. This approach offers thus a way to electrically control the magnetization of the ferromagnet when it is magnetically coupled to the multiferroic [29]. This indirect coupling has been widely studied in the last few years, by developing devices with well-engineered interfaces and hopefully higher magnetoelectric coupling effects at room temperature than with intrinsic multiferroics.

Electric field control of exchange bias, magnetic anisotropy and/or magnetic switching have been demonstrated in multiferroic heterostructures using BFO [105], $YMnO_3$ [106,107] and $LuMnO_3$ [108] as ferroelectric antiferromagnetic materials. The magnetization control with electric field is mediated by a collinear coupling between the magnetization in the ferromagnet and the projection of the antiferromagnetic order in the multiferroic. As an example, domain matching of the ferroelectric and ferromagnetic domains has been observed and switched in CoFe/BFO heterostructures [109,100,30]. Out of plane switching of the $BiFeO_3$ polarization gives rise to a rotation of the antiferromagnetic order, affecting the magnetization of the CoFe layer via the exchange bias effect on the BFO/CoFe interface [109] (Fig. 12a and b). In a different and specific geometry, Heron et al. achieved a 180° reversal of the CoFe magnetization thanks to the net 180° in plane switching of the $BiFeO_3$ [100]. In this case, one to one magnetic interface coupling of the stripy domains is illustrated (Fig. 12c and d) and is responsible for the electrical full reversal of the magnetization. Recently, You and co-workers have added one more level

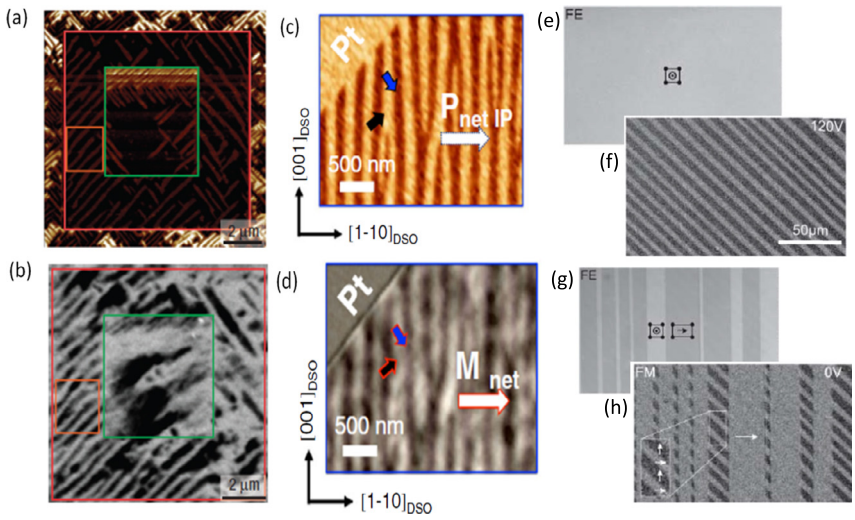

Fig. 12. (Color online.) Electric control of magnetization by magnetoelectric coupling at ferromagnet/multiferroic interface. Switching of ferroelectric domains in electrically written BFO areas (PFM picture (a)) and direct matching with the magnetic domain structure of a CoFe film grown on BFO (XMCD-PEEM picture (b)) (after Chu et al. [109]). Another study revealing the one-to-one mapping of the ferroelectric domains of BFO (PFM picture (c)) and the ferromagnetic domains of CoFe (XMCD-PEEM picture (d)) (after Heron et al. [100]). Ferroelectric switching in $BaTiO_3$ domains coupled via strain with the magnetic domains in $Co_{0.9}Fe_{0.1}$: Optical microscopy of the ferroelectric domains in the $BaTiO_3$ crystal (birefringent contrast): (e) $BaTiO_3$ poled under 120 V leading to single domain formation, (g) $BatiO_3$ relaxed with no bias applied leading to multidomain relaxation. Corresponding optical microscopy (f, h) of the ferromagnetic domains (magneto-optical Kerr effect contrast) in the coupled CoFe thin film (after Lahtinen et al. [111]).

of complexity to the interfacial magnetic coupling by observing that magnetic anisotropy of top $La_{0.7}Sr_{0.3}MnO_3$ thin film can be fully driven by the ferroelectric domain configuration of underneath $BiFeO_3$ [110]. They showed that in addition to the magnetic coupling at the ferromagnet/antiferromagnet interface, a uniaxial magnetic anisotropy in LSMO films is also (if not only) induced by the anisotropic tensile strain imposed by the BFO distorted cells (corresponding to a FE variant). This strain mediated magneto-electric coupling can also be observed in bi-materials stacks involving no multiferroic and no antiferromagnet as for instance with $Co_{0.9}Fe_{0.1}$ deposited on top of $BaTiO_3$ bulk crystals [111]. Here the FE domain structure in $BaTiO_3$ can be tuned with an electric field allowing controlling the lateral domain growth and shrinking when field goes back to zero. The magnetic domain pattern in $Co_{0.9}Fe_{0.1}$ strictly follows the underlying FE pattern when the electric field is changed (Fig. 12e–h). The coupling is in this case purely strain mediated and leads to an electric field induced 90° rotation of the magneto-elastic axis.

These results are promising but also highlight the complexity of the magnetoelectric coupling at the interface between a ferromagnet and a multiferroic due to the strong interplay between ferroelastic, ferroelectric and antiferromagnetic orders in the multiferroic [112]. Strain-mediated, charge-mediated and spin exchange magnetoelectric couplings can come into play [29]. In this context, disentangling their influence on the electric control of magnetization is a prerequisite for controlling and designing functional magnetoelectric devices.

3.4. Conclusion

The maturity and availability of various co-microscopy techniques now allow the direct visualization of ferroelectric and ferromagnetic domains at the nanoscale in thin films heterostructures. This capability opens a new playground to observe and understand the nature of the coupling between domains related to different orders: it allows intrinsic coupling as well as interfacial coupling to be investigated. Tremendous progresses have been achieved through the past decade and allow robust full switching (180°) of one order thanks to the other. Obtaining such a “Grail” is indeed a great step forward but interfacial magnetoelectric coupling remains obviously complex and will need intense labor to be deeply understood. Finally, almost nothing is known about the dynamic properties of coupled domain walls. This opened question has to be addressed in a near future.

Acknowledgements

This work received financial support from the European Research Council Advanced Grant FEMMES (contract No. 267579) and French Agence Nationale de la Recherche (ANR) through the project MULTIDOLLS.

References

[1] S. Parkin, M. Hayashi, L. Thomas, Science 320 (2008) 190.

[2] A. Chanthbouala, et al., Nat. Phys. 7 (2011) 626.
[3] A. Chanthbouala, et al., Nat. Mater. 11 (2012) 860.
[4] J. Seidel, et al., Nat. Mater. 8 (2009) 229.
[5] Q. He, et al., Phys. Rev. Lett. 108 (2012) 067203.
[6] J. Seidel, et al., Phys. Rev. Lett. 107 (2011) 126805.
[7] C. Kittel, Phys. Rev. B 70 (1946) 965.
[8] A.L. Roitburd, Phys. Status Solidi A 37 (1976) 329.
[9] W. Pompe, et al., J. Appl. Phys. 74 (1993) 6012.
[10] J.S. Speck, W. Pompe, J. Appl. Phys. 76 (1994) 466.
[11] N.A. Pertsev, A.G. Zembilgotov, J. Appl. Phys. 78 (1995) 6170.
[12] M. Daraktchiev, et al., Ferroelectrics 375 (2008) 122.
[13] E. Chu, et al., Adv. Mater. 18 (2006) 2307.
[14] L.W. Martin, et al., Nano Lett. 8 (2008) 2050.
[15] E. Chu, et al., Nano Lett. 9 (2009) 1726.
[16] E. Chen, et al., Appl. Phys. Lett. 104 (2014) 182908.
[17] E. Chu, et al., Adv. Mater. 19 (2007) 2662.
[18] G. Catalan, et al., Rev. Mod. Phys. 84 (2012) 119.
[19] G. Catalan, et al., J. Phys. Condens. Matter 19 (2007) 022201.
[20] G. Catalan, et al., J. Phys. Condens. Matter 19 (2007) 132201.
[21] G. Catalan, et al., J. Mater. Sci. 44 (2009) 5307.
[22] G. Catalan, J.F. Scott, Adv. Mater. 21 (2009) 2463.
[23] J.F. Scott, J. Phys. Condens. Matter 18 (2006) R361.
[24] A. Schilling, et al., Phys. Rev. B 74 (2006) 024115.
[25] A. Schilling, et al., Nano Lett. 9 (2009) 3359.
[26] G. Catalan, et al., Phys. Rev. Lett. 100 (2008) 027602.
[27] T.H.E. Lahtinen, et al., Adv. Mater. 23 (2011) 3187.
[28] T.H.E. Lahtinen, et al., Appl. Phys. Lett. 102 (2013) 112406.
[29] C.A.F. Vaz, J. Phys. Condens. Matter 24 (2012) 333201.
[30] M. Trassin, et al., Phys. Rev. B 87 (2013) 134426.
[31] M.R. Scheinfein, Rev. Sci. Instrum. 61 (1990) 2501.
[32] T. Zhao, et al., Nat. Mater. 5 (2006) 823.
[33] A. Tagantsev, et al., Domains in Ferroic Crystals and Thin Films, Springer, New York, 2010.
[34] H. Fu, et al., Phys. Rev. Lett. 91 (2003) 257601.
[35] I. Naumov, et al., Nature 432 (2004) 737.
[36] I. Kornev, et al., Phys. Rev. Lett. 93 (2004) 196104.
[37] I. Ponomareva, et al., Phys. Rev. B 72 (2005) 214118.
[38] S. Prosandeev, et al., Phys. Rev. Lett. 96 (2006) 237601.
[39] S. Prosandeev, et al., Phys. Rev. B 75 (2007) 094102.
[40] S. Prosandeev, et al., J. Phys. Condens. Matter 20 (2008) 193201.
[41] J.M. Gregg, Ferroelectrics 433 (2012) 74.
[42] L.J. McGilly, et al., Nano Lett. 10 (2010) 4200.
[43] L.J. McGilly, et al., Appl. Phys. Lett. 98 (2011) 132902.
[44] R.G.P. McQuaid, et al., Nat. Commun. 2 (2011) 404.
[45] L.J. McGilly, J.M. Gregg, Nano Lett. 11 (2011) 4490.
[46] L.-W. Chang, et al., Nano Lett. 13 (2013) 2553.
[47] A. Gruverman, et al., J. Phys. Condens. Matter 20 (2008) 342201.
[48] B.J. Rodriguez, et al., Nano Lett. 9 (2009) 1127.
[49] Y. Ivry, et al., Phys. Rev. Lett. 104 (2010) 207602.
[50] C.-L. Jia, et al., Science 331 (2011) 1420.
[51] C.T. Nelson, et al., Nano Lett. 11 (2011) 828.
[52] Y. Qi, et al., J. Appl. Phys. 111 (2012) 104117.
[53] A. Berger, et al., Phys. Rev. B 85 (2012) 064104.
[54] C.J. Fennie, K.M. Rabe, Phys. Rev. B 72 (2005) 100103(R).
[55] B.B. Van Aken, et al., Nat. Mater. 3 (2004) 164.
[56] M. Fiebig, et al., Nature 419 (2002) 818.
[57] T. Lottermoser, et al., Nature 430 (2004) 541.
[58] S. Artyukhin, et al., Nat. Mater. 13 (2014) 42.
[59] T. Jungk, et al., Appl. Phys. Lett. 97 (2010) 012904.
[60] T. Choi, et al., Nat. Mater. 9 (2010) 253.
[61] Q. Zhang, et al., Sci. Rep. 3 (2013) 2741.
[62] E.B. Lochocki, et al., Appl. Phys. Lett. 99 (2011) 232901.
[63] Y. Geng, et al., Nano Lett. 12 (2012) 6055.
[64] Y. Geng, et al., Nat. Mater. 13 (2014) 163.
[65] J. Li, et al., Phys. Rev. B 87 (2013) 094106.
[66] S.C. Chae, et al., Phys. Rev. Lett. 108 (2012) 167603.
[67] Y. Kumagai, N.A. Spaldin, Nat. Commun. 4 (2013) 1540.
[68] X. Wang, et al., Phys. Rev. Lett. 112 (2014) 247601.
[69] R.K. Vasudevan, et al., Adv. Funct. Mater. 23 (2013) 2592.
[70] J. Privratska, V. Janovec, Ferroelectrics 222 (1999) 23.
[71] A. Lubk, et al., Phys. Rev. B 80 (2009) 104110.
[72] J. Seidel, et al., Phys. Rev. Lett. 105 (2010) 197603.
[73] P. Maksymovych, et al., Nano Lett. 11 (2011) 1906.
[74] P. Maksymovych, et al., Nano Lett. 12 (2012) 209.
[75] S. Farokhipoor, B. Noheda, Phys. Rev. Lett. 107 (2011) 127601.

[76] S. Farokhipoor, B. Noheda, J. Appl. Phys. 112 (2012) 052003.
[77] N. Balke, et al., Nat. Phys. 8 (2012) 81.
[78] M. Schröder, et al., Adv. Funct. Mater. 22 (2012) 3936.
[79] R. Palai, et al., Phys. Rev. B 77 (2008) 014110.
[80] I. Stolichnov, et al., Appl. Phys. Lett. 104 (2014) 132902.
[81] J. Guyonnet, et al., Adv. Mater. 23 (2011) 5377.
[82] T. Sluka, et al., Nat. Commun. 4 (2013) 1808.
[83] W. Wu, et al., Phys. Rev. Lett. 108 (2012) 077203.
[84] D. Meier, et al., Nat. Mater. 11 (2012) 284.
[85] M. Daraktchiev, G. Catalan, J.F. Scott, Phys. Rev. B 81 (2010) 224118.
[86] J.X. Zhang, et al., Nanoscale 4 (2012) 6196.
[87] Y. Tokura, S. Seki, Adv. Mater. 22 (2010) 1554.
[88] Y. Tokunaga, et al., Phys. Rev. Lett. 112 (2014) 037203.
[89] K.F. Wang, J.-M. Liu, Z.F. Ren, Adv. Phys. 58 (2009) 321.
[90] W. Wang, et al., Phys. Rev. Lett. 110 (2013) 237601.
[91] N. Balke, et al., Nat. Nanotechnol. 4 (2009) 868.
[92] R.K. Vasudevan, et al., ACS Nano 5 (2011) 879.
[93] R.K. Vasudevan, et al., Nat. Commun. 5 (2014) 4971.
[94] S. Matzen, et al., Nat. Commun. 5 (2014) 4415.
[95] M.Y. Gureev, A.K. Tagantsev, N. Setter, Phys. Rev. B 83 (2011) 184104.
[96] E.A. Eliseev, et al., Phys. Rev. B 83 (2011) 235313.
[97] R.K. Vasudevan, et al., Nano Lett. 12 (2012) 5524.
[98] M.-G. Han, et al., Adv. Mater. 25 (2013) 2415.
[99] D. Lebeugle, et al., Phys. Rev. Lett. 100 (2008) 227602.
[100] J.T. Heron, et al., Phys. Rev. Lett. 107 (2011) 217202.
[101] S. Seki, et al., Science 336 (2012) 198.
[102] D.M. Evans, et al., Nat. Commun. 4 (2013) 1534.
[103] J. Schiemer, et al., Adv. Funct. Mater. 24 (2014) 2993.
[104] H. Béa, et al., Phys. Rev. Lett. 100 (2008) 017204.
[105] J. Allibe, et al., Nano Lett. 12 (2012) 1141.
[106] V. Laukhin, et al., Phys. Rev. Lett. 97 (2006) 227201.
[107] J.W. Wang, et al., Appl. Phys. Lett. 102 (2013) 102906.
[108] V. Skumryev, et al., Phys. Rev. Lett. 106 (2011) 057206.
[109] Y.-H. Chu, et al., Nat. Mater. 7 (2008) 47.
[110] L. You, et al., Phys. Rev. B 88 (2013) 184426.
[111] T.H.E. Lahtinen, K.J.A. Franke, S. van Dijken, Sci. Rep. 2 (2012) 258.
[112] J.J. Wang, et al., Sci. Rep. 4 (2014) 4553.